

International Journal of Modern Physics B
 © World Scientific Publishing Company

THE TRANSPORT OF SELF-PROPELLED ELLIPSOIDAL PARTICLES CONFINED IN 2D SMOOTH CORRUGATED CHANNEL

BING WANG

*School of Mechanics and Optoelectronic Physics, Anhui University of Science and Technology
 Huainan, 232001, P.R.China
 hnitwb@163.com*

WENFEI WU

*School of Mechanics and Optoelectronic Physics, Anhui University of Science and Technology
 Huainan, 232001, P.R.China*

Received Day Month Year

Revised Day Month Year

Directed transport of self-propelled ellipsoidal particles confined in a smooth corrugated channel with asymmetric potential and Gaussian colored noise is investigated. Effects of the channel, potential and colored noise on the system are discussed. Large x axis noise intensity inhibits the transport in $-x$ and $+x$ direction. The directed transport speed $|\langle V \rangle|$ has a maximum with increasing y axis noise intensity. Proper size of the bottleneck is good for the directed transport of the ellipsoidal particles, but large and small size of bottleneck inhibits this directed transport. The transport reverse phenomenon appears with increasing load and self-propelled speed. Perfect sphere particle is easier to directed transport than needlelike ellipsoid particle.

Keywords: Self-Propelled Ellipsoidal Particle; Confined Channel; Directed Transport.

1. Introduction

Recent years, we have seen enormous activities in the study of the properties of the confined Brownian particles. These studies, both theoretical and experimental, revealed that there are two ways of confinement fundamentally effect a system. One way is by regulating the transport space accessible to its diffusing components,¹ and the other way is by increasing the hydrodynamic drag on the particles.² There exists a large number of natural and artificial confined geometries, e.g., biological cells,³⁻⁶ zeolites,⁷ artificial nanopores,^{8,9} ionpumps¹⁰⁻¹³ and micro fluidic devices.¹⁴⁻¹⁷

Confined particle shows a series of novel features, e.g. current reversal,¹⁸⁻²² self-organization,^{23,24} geometry-induced stochastic resonance phenomenon^{25,26} and so on. Hänggi *et al.* proposed a model of asymmetry particles confined in a compartmentalized channel and found the absolute negative mobility.²⁷ Ghosh *et al.* investigated directed transport of suspended particles and found inertial corrections must

be considered when the width of the bottlenecks is smaller than an appropriate particle diffusion length.²⁸ Using the hybrid molecular dynamics method, Chen *et al.* studied the properties of self-propelled synthetic motors.²⁹ Pu *et al.* investigated the reentrant phase separation behavior of active particles and found that phase separation shows a re-entrance behavior with variation of the interaction strength.³⁰ Li *et al.* found non-Gaussian normal diffusion phenomenon of Brownian particles floating in a narrow corrugated channel with fluctuating cross section.³¹ Yang *et al.* experimentally investigated the diffusion of particles moving in a planar channel.³²

In many biological systems, transport particles are often nonspherical, such as proteins diffusing in membranes and fine grains migrating through the pores of micro media.^{33,34} Han *et al.* studied the transport of ellipsoid particles confined in a two dimensional channel and quantified the crossover from short-time anisotropic to long-time isotropic diffusion.³⁵ Ohta *et al.* found deformable particles exhibit bifurcation and circular motion phenomenon.³⁶ Ai *et al.* investigated the rectified transport of active ellipsoidal particles in a two-dimensional asymmetric potential.³⁷ Ghosh *et al.* numerically simulated the transport of elliptic particles confined in two-dimensional channels with reflecting walls and observed long diffusion transients.³⁸ Traditionally, stochastic differential equations used in physical and biological science have involved Gaussian white noise. Investigation of laser noise problems,^{39,40} bistable systems⁴¹ and self-propelled particle systems^{42,43} found that it is necessary to consider colored noise in those systems.

In this paper, we investigate the directed transport of self-propelled ellipsoidal Brownian particles confined in a two dimensional(2D) smooth channel. The paper is organized as follows: The basic model of the system is provided in Sect.2. In Sect.3, the effects of the channel, the potential and the colored noise on the ellipsoidal particles are investigated by means of simulations. In Sect. 4, we get the conclusions.

2. Basic model and methods

In this work, we consider self-propelled ellipsoidal particles confined in a 2D smooth corrugated channel with potential and Gaussian colored noise. In the lab frame, the displacement $\delta\vec{R}(t)$ of the particle can be described by the mass center($\delta x, \delta y$). We use the following Langevin equations to describe the dynamics of the particle^{35,44}

$$\frac{\partial x}{\partial t} = v_0 \cos \theta(t) + F_x[\bar{\Gamma} + \Delta\Gamma \cos 2\theta(t)] + \Delta\Gamma F_y \sin 2\theta(t) + \xi_x(t), \quad (1)$$

$$\frac{\partial y}{\partial t} = v_0 \sin \theta(t) + F_y[\bar{\Gamma} - \Delta\Gamma \cos 2\theta(t)] + \Delta\Gamma F_x \sin 2\theta(t) + \xi_y(t), \quad (2)$$

$$\frac{\partial \theta(t)}{\partial t} = \xi_\theta(t). \quad (3)$$

THE TRANSPORT OF SELF-PROPELLED ELLIPSOIDAL PARTICLES CONFINED IN 2D SMOOTH CORRUGATED CHANNEL

The angle between the lab frame x axis and the body frame \hat{x} axis is $\theta(t)$. The self-propelled velocity is v_0 , and v_0 is along the long axis of the particle. The quantities $\bar{\Gamma} = \frac{1}{2}(\Gamma_x + \Gamma_y)$ and $\Delta\Gamma = \frac{1}{2}(\Gamma_x - \Gamma_y)$ are the average and difference mobilities of the body, respectively. The mobilities along its long axis and short axis are Γ_x and Γ_y , respectively. $\Delta\Gamma$ determines the asymmetry of the body of the ellipsoidal particle. The particle is a perfect sphere when $\Delta\Gamma = 0$ and a very needlelike ellipsoid when $\Delta\Gamma \rightarrow \bar{\Gamma}$. ξ_x , ξ_y and ξ_θ are the noises. ξ_x and ξ_y parallel to x axis and y axis, respectively. ξ_θ is the angle noise. ξ_x , ξ_y and ξ_θ satisfy the following relations,

$$\langle \xi_i(t) \rangle = 0, (i = x, y, \theta), \quad (4)$$

$$\langle \xi_i(t) \xi_j(t') \rangle = \delta_{ij} \frac{Q_i}{\tau_i} \exp[-\frac{|t-t'|}{\tau_i}], (i = x, y, \theta), \quad (5)$$

where Q_i and τ_i are the noise intensity and the self-correlation time of the noises, respectively.

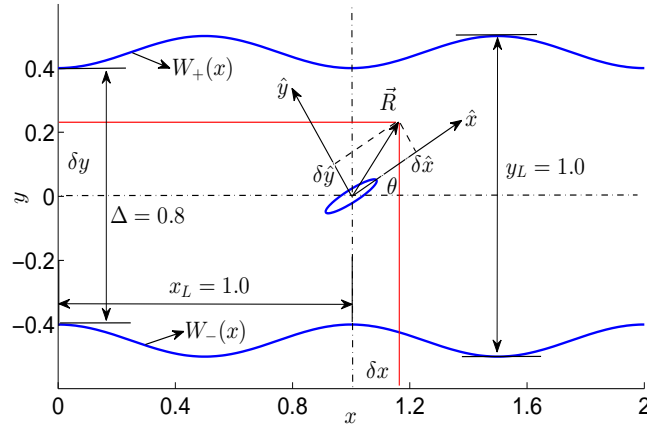


Fig. 1. Illustrations of the smooth corrugated channel with $\Delta = 0.8$, $x_L = y_L = 1.0$, $\eta = 2.0$.

The particles are confined in a two dimensional smooth corrugated channel. As shown in Fig.1, the channel is consisted of many cavities and is periodic in spatial along the x -axis. The walls of the cavity are modeled by the following sinusoidal functions,⁴⁵

$$W_+(x) = \frac{1}{2}[\Delta + (y_L - \Delta) \sin^\eta(\frac{\pi x}{x_L})], \quad (6)$$

4 BING WANG

$$W_-(x) = -\frac{1}{2}[\Delta + (y_L - \Delta) \sin^\eta(\frac{\pi x}{x_L})], \quad (7)$$

where $x_L = 1.0$ and $y_L = 1.0$ are the length and width of the cavity, respectively. The additional tunable geometric parameter is η . The cavity represents the compartment of sinusoidally corrugated channel when $\eta = 2$. When $\eta \rightarrow 0$, the cavity reproduces the compartment of sharply corrugated channels. The channel width is $h(x) = W_+ - W_-$. The minimal channel width(the bottleneck) is $h_{min} = h(x)|_{x=\pm k, k=0,1,2,\dots} = \Delta$, and through which the particles can exit the cavity. The maximal channel width is $h_{max} = h(x)|_{x=\pm(2k+1)\frac{1}{2}, k=0,1,2,\dots} = y_L$.

The asymmetric potential is described by the following equation³⁷(shown in Fig.2),

$$U(x, y) = \frac{U_0}{2}y^2[\cos(x + \varepsilon \ln \cosh y) + 1.1] + fx, \quad (8)$$

where U_0 is the height of the potential, and f is the load. The asymmetric parameter of the potential is ε , and the potential is symmetric for $\varepsilon = 0.0$. The equipotential is look like a herringbone pattern if $\varepsilon \neq 0$. The forces $F_x = -\frac{\partial U}{\partial x}$ and $F_y = -\frac{\partial U}{\partial y}$ are along x and y directions of the lab frame, respectively.

In the theory of Brownian motion, the central question is the particle's over all long time behavior. The velocity of the particle is one of the key quantities. We only calculate the average velocity in x direction because the channel in y direction is confined,

$$\langle V_{\theta_0} \rangle = \lim_{t \rightarrow \infty} \frac{\langle x(t) - x(t_0) \rangle}{t - t_0}, \quad (9)$$

the position of particles at time t_0 is $x(t_0)$. The initial angle of the trajectory is θ_0 . The full average velocity after another average over all θ_0 is

$$\langle V \rangle = \frac{1}{2\pi} \int_0^{2\pi} \langle V_{\theta_0} \rangle d\theta_0. \quad (10)$$

3. Results and discussion

In order to give a simple and clear analysis of the system. We integrate Eqs.(1,2,3) with time step $\Delta t = 10^{-4}$ using the Euler algorithm. The average velocity is obtained as ensemble averages over 10^5 trajectories with random initial conditions. In the simulation, we set $x_L = y_L = 1.0$, $\bar{\Gamma} = 1.0$ and $U_0 = 1.0$ throughout the paper.

Fig.3 displays the average velocity $\langle V \rangle$ as a function of x axis noise intensity Q_x with different load f . In this paper, we find the average velocity $\langle V \rangle > 0$, and $\langle V \rangle$ decreases with increasing Q_x when the load $f = -0.1$ and $f = -0.3$. Which means that negative load f induces directed transport in $+x$ direction, and large x axis noise intensity Q_x inhibits this transport. When the load $f > 0$ ($f = 0.1$ and $f = 0.3$), the average velocity $\langle V \rangle < 0$, and $\langle V \rangle$ increases with increasing Q_x . So positive f leads to directed transport in $-x$ direction, and large Q_x is bad for this directed transport. Of cause, we can also say that the directed transport speed

THE TRANSPORT OF SELF-PROPELLED ELLIPSOIDAL PARTICLES CONFINED IN 2D SMOOTH CORRUGATED CHANNEL

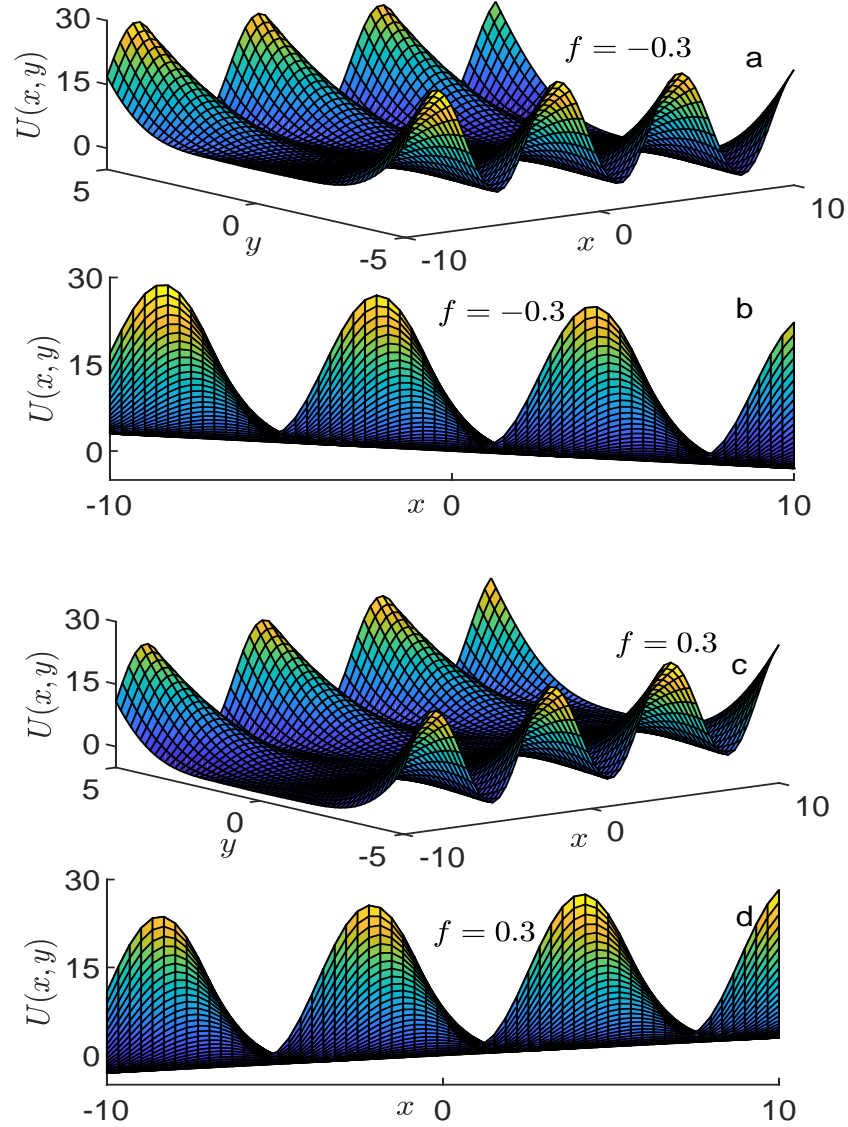


Fig. 2. The asymmetric potential $U(x, y)$ with $U_0 = 1.0$, $\varepsilon = 0.5$:(a)3D view with $f = -0.3$;(b)Front view with $f = -0.3$; (c)3D view with $f = 0.3$; (d)Front view with $f = 0.3$.

$|\langle V \rangle|$ (the absolute value of $\langle V \rangle$) decreases with increasing Q_x , so large x axis noise intensity inhabits directed transport along x axis.

Fig.4 displays $\langle V \rangle$ as a function of self-correlation time τ_x with different load f . In this figure, comparing with the effect of Q_x in Fig.3, we find τ_x has exactly reverse

6 BING WANG

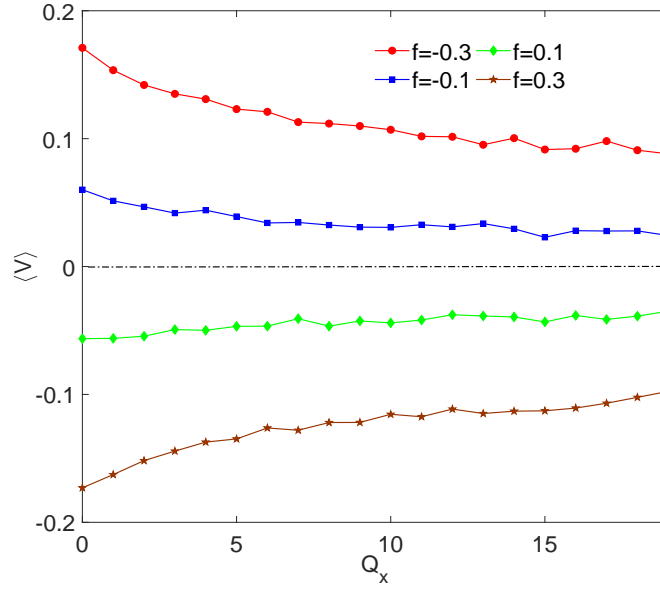


Fig. 3. The average velocity $\langle V \rangle$ as a function of Q_x for different values of f . The other parameters are $\Delta = 0.8$, $\varepsilon = 0.5$, $\eta = 2.0$, $v_0 = 0.5$, $Q_x = Q_y = Q_\theta = 1.0$, $\tau_x = \tau_y = \tau_\theta = 1.0$.

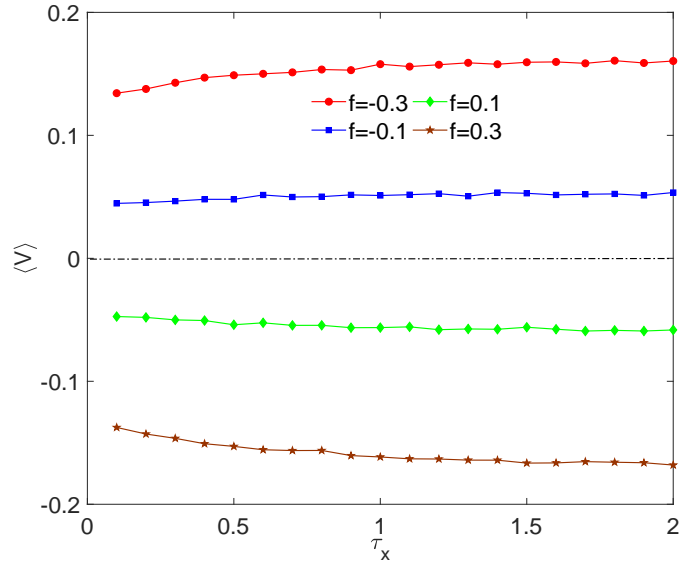


Fig. 4. The average velocity $\langle V \rangle$ as a function of τ_x for different values of f . The other parameters are $\Delta = 0.8$, $\varepsilon = 0.5$, $\eta = 2.0$, $v_0 = 0.5$, $Q_x = Q_y = Q_\theta = 1.0$, $\tau_y = \tau_\theta = 1.0$.

effect on the system. The directed transport speed $|\langle V \rangle|$ increases with increasing τ_x . Large self-correlation time τ_x is good for the transport. In this figure, we can also find negative f induces directed transport in $+x$ direction, but positive f induces directed transport in $-x$ direction. From Figs. 3 and 4, we find the slopes of $\langle V \rangle - Q_x$ and $\langle V \rangle - \tau_x$ curves almost changes to zero when Q_x and τ_x are large. So changes of Q_x and τ_x have weak impact on the transport when their values are large.

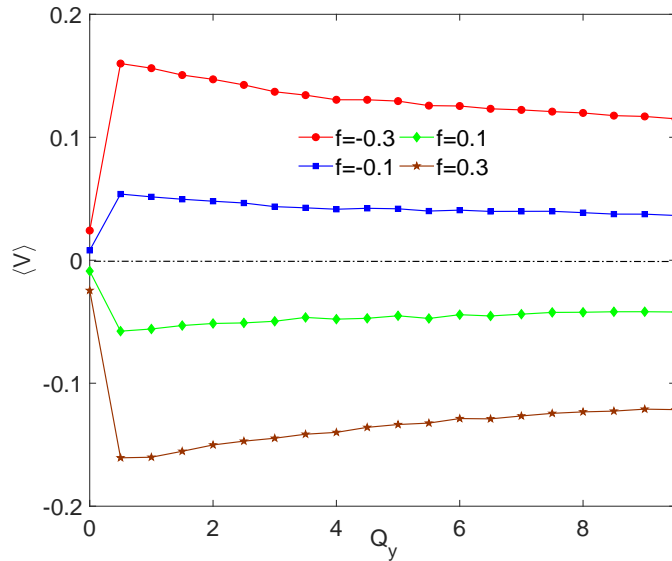


Fig. 5. The average velocity $\langle V \rangle$ as a function of Q_y for different values of f . The other parameters are $\Delta = 0.8$, $\varepsilon = 0.5$, $\eta = 2.0$, $v_0 = 0.5$, $Q_x = Q_\theta = 1.0$, $\tau_x = \tau_y = \tau_\theta = 1.0$.

Fig.5 displays $\langle V \rangle$ as a function of y axis noise intensity Q_y with different f . In this figure, we find the directed transport speed $|\langle V \rangle|$ has a maximum with increasing Q_y . So proper y axis noise intensity is good for the transport in x and $-x$ direction, but too large or too small Q_y inhabits this phenomenon. From figures 3 and 5, we find an interesting phenomenon, large x axis noise intensity inhabits the directed transport in $+x$ and $-x$ direction, but proper y axis noise intensity is good for this transport.

Fig.6 displays $\langle V \rangle$ as a function of y axis noise self-correlation time τ_y for different f . Comparing with the effect of τ_x in Fig.4, we find the directed transport speed $|\langle V \rangle|$ decreases with increasing τ_y . This means that large τ_y has negative effect on the transport along x axis.

Figs.7 and 8 display $\langle V \rangle$ as functions of angle noise intensity Q_θ and self-correlation time τ_θ for different f , respectively. In these two figures, we find there exists almost no change of $\langle V \rangle$ with increasing Q_θ and τ_θ . So the effect of the angle

8 BING WANG

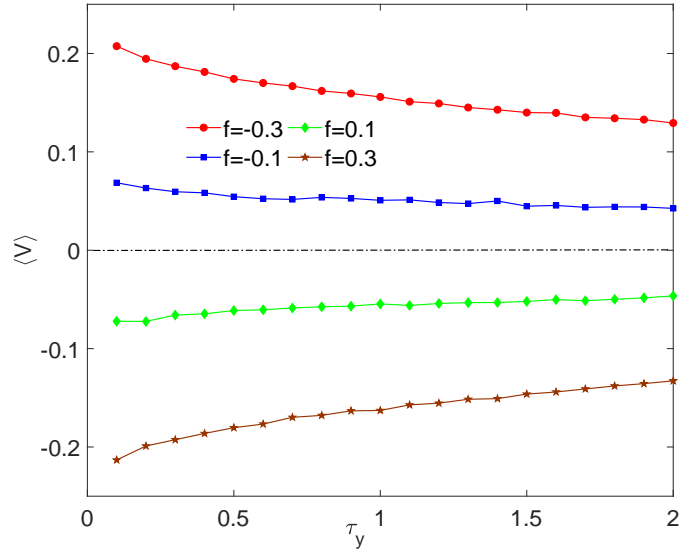


Fig. 6. The average velocity $\langle V \rangle$ as a function of τ_y for different values of f . The other parameters are $\Delta = 0.8$, $\varepsilon = 0.5$, $\eta = 2.0$, $v_0 = 0.5$, $Q_x = Q_y = Q_\theta = 1.0$, $\tau_x = \tau_\theta = 1.0$.

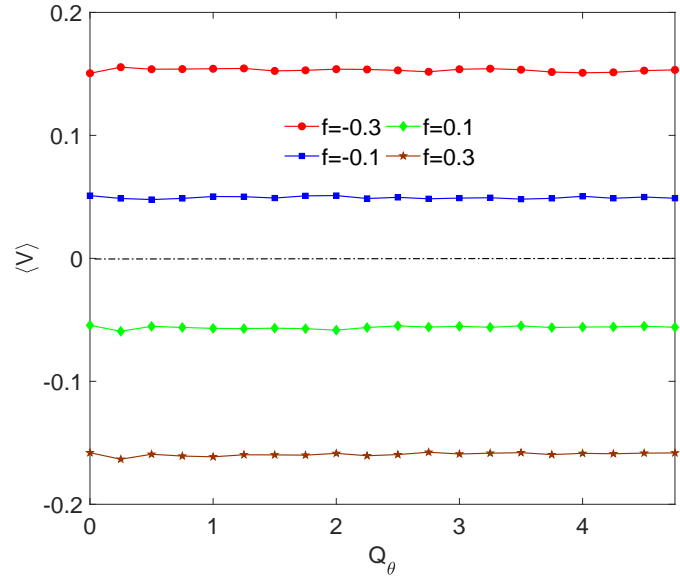


Fig. 7. The average velocity $\langle V \rangle$ as a function of Q_θ for different values of f . The other parameters are $\Delta = 0.8$, $\varepsilon = 0.5$, $\eta = 2.0$, $v_0 = 0.5$, $Q_x = Q_y = 1.0$, $\tau_x = \tau_y = \tau_\theta = 1.0$.

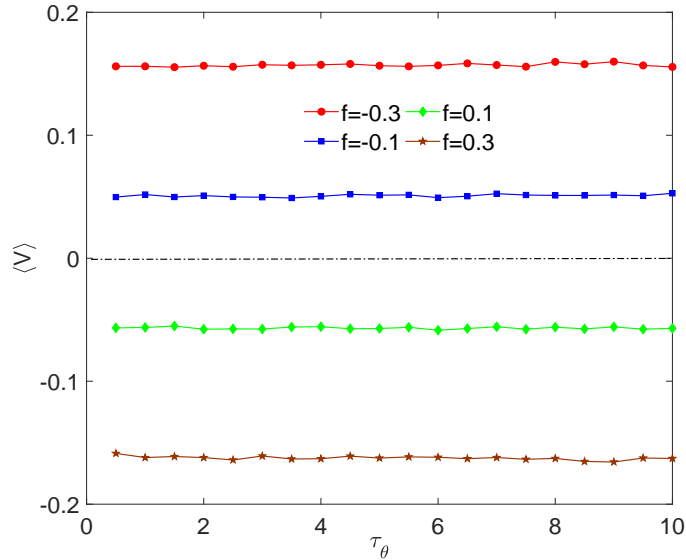


Fig. 8. The average velocity $\langle V \rangle$ as a function of τ_θ for different values of f . The other parameters are $\Delta = 0.8$, $\varepsilon = 0.5$, $\eta = 2.0$, $v_0 = 0.5$, $Q_x = Q_y = Q_\theta = 1.0$, $\tau_x = \tau_y = 1.0$.

noise is very weak for the transport.

The average velocity $\langle V \rangle$ as a function of the bottleneck (the minimal channel width) Δ is reported in Fig.9. We find $\langle V \rangle \rightarrow 0$ when $\Delta \rightarrow 0$. This is because the channel becomes many closed cavities when $\Delta \rightarrow 0$, and the particle is confined in these cavities. The directed transport speed $|\langle V \rangle|$ increases with increasing Δ , and reaches a maximum when $\Delta = 1$, and then decreases with increasing Δ . So an interesting phenomena appears, that is, large and small size of the bottleneck both restrains the directed transport.

The average velocity $\langle V \rangle$ as a function of the asymmetry of the body $\Delta\Gamma$ for different f is reported in Fig.10. We know $\Delta\Gamma$ characterizes the asymmetry of the particle, and the particle is a perfect sphere when $\Delta\Gamma = 0$, and the particle is a very needlelike ellipsoid when $\Delta\Gamma \rightarrow \bar{\Gamma}$. In this figure, we find the average directed transport speed $|\langle V \rangle|$ decreases with increasing $\Delta\Gamma$. So perfect sphere particle is more easier for directed transport than needlelike ellipsoid particle. This result coincides with the common sense.

The average velocity $\langle V \rangle$ as a function of the asymmetric parameter ε for different f is reported in Fig.11. We find the $\langle V \rangle - \varepsilon$ curve is almost horizontal, this means that the effect of ε is very weak on the directed transport phenomenon.

The average velocity $\langle V \rangle$ as a function of self-propelled speed v_0 with different f is reported in Fig.12. When the load is negative ($f = -0.3$ and $f = -0.1$), inert particle (self-propelled speed $v_0 = 0$) moves in $+x$ direction ($\langle V \rangle > 0$), and $\langle V \rangle$

10 BING WANG

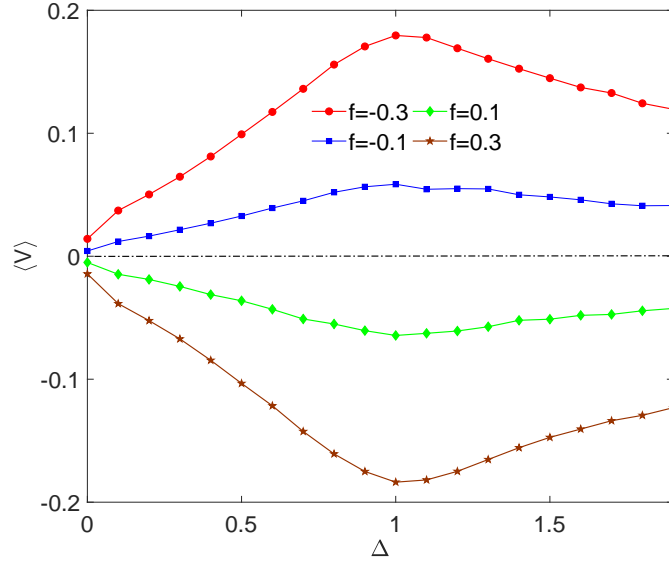


Fig. 9. The average velocity $\langle V \rangle$ as a function of the size of bottleneck Δ for different values of f . The other parameters are $\varepsilon = 0.5$, $\eta = 2.0$, $v_0 = 0.5$, $Q_x = Q_y = Q_\theta = 1.0$, $\tau_x = \tau_y = \tau_\theta = 1.0$.

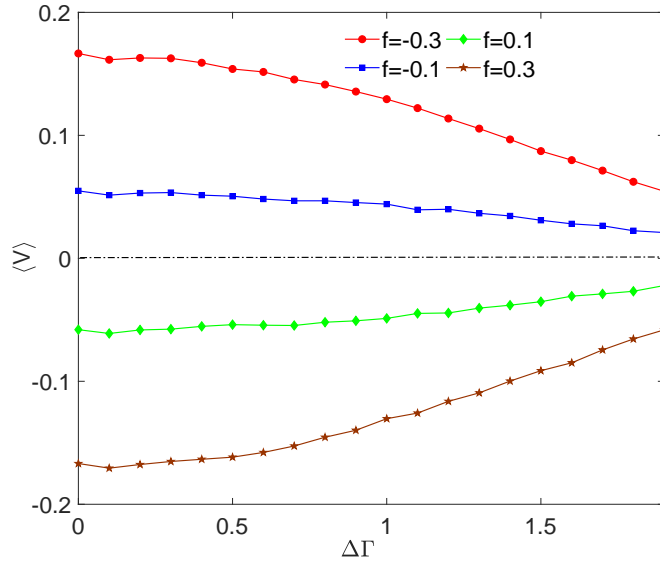


Fig. 10. The average velocity $\langle V \rangle$ as a function of $\Delta\Gamma$ for different values of f . The other parameters are $\Delta = 0.8$, $\varepsilon = 0.5$, $\eta = 2.0$, $v_0 = 0.5$, $Q_x = Q_y = Q_\theta = 1.0$, $\tau_x = \tau_y = \tau_\theta = 1.0$.

THE TRANSPORT OF SELF-PROPELLED ELLIPSOIDAL PARTICLES CONFINED IN 2D SMOOTH CORRUGATED CHANNEL

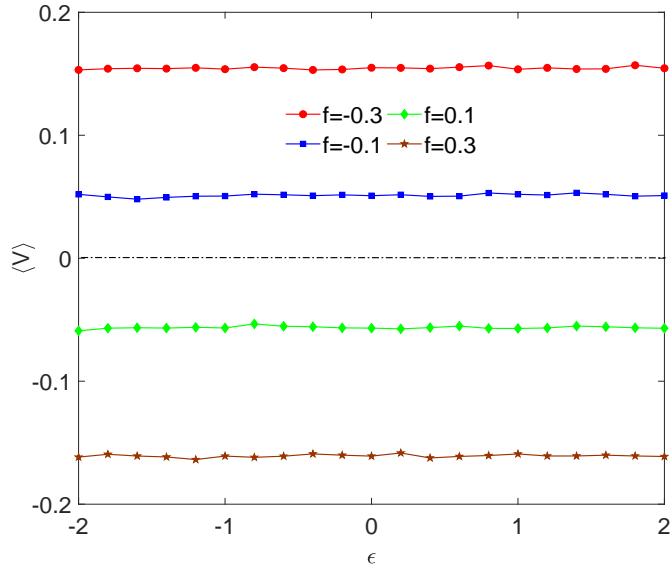


Fig. 11. The average velocity $\langle V \rangle$ as a function of ϵ for different values of f . The other parameters are $\Delta = 0.8$, $\eta = 2.0$, $v_0 = 0.5$, $Q_x = Q_y = Q_\theta = 1.0$, $\tau_x = \tau_y = \tau_\theta = 1.0$.

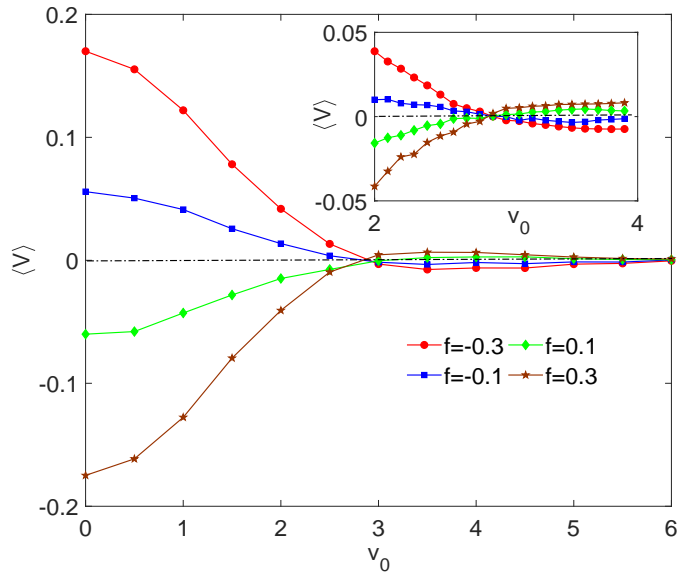


Fig. 12. The average velocity $\langle V \rangle$ as a function of self-propelled speed v_0 for different values of f . The other parameters are $\Delta = 0.8$, $\epsilon = 0.5$, $\eta = 2.0$, $Q_x = Q_y = Q_\theta = 1.0$, $\tau_x = \tau_y = \tau_\theta = 1.0$.

decreases with increasing v_0 , then the particles changes to moving in $-x$ direction when $2.8 < v_0 < 6.0$, and $\langle V \rangle \rightarrow 0$ when $v_0 = 6.0$. So the transport reverse phenomenon appears with increasing v_0 . When the load is positive($f = 0.1$ and $f = 0.3$), inert particle($v_0 = 0$) moves in $-x$ direction($\langle V \rangle < 0$), and the transport reverse phenomenon appears too with increasing v_0 , and $\langle V \rangle \rightarrow 0$ when $v_0 = 6.0$. In this figure, we can also find negative load leads to directed transport in $+x$ direction when $v_0 < 3$, but positive load leads to directed transport in $-x$ direction when $v_0 < 3$. So self-propelled speed v_0 can also influence the moving direction of the particles.

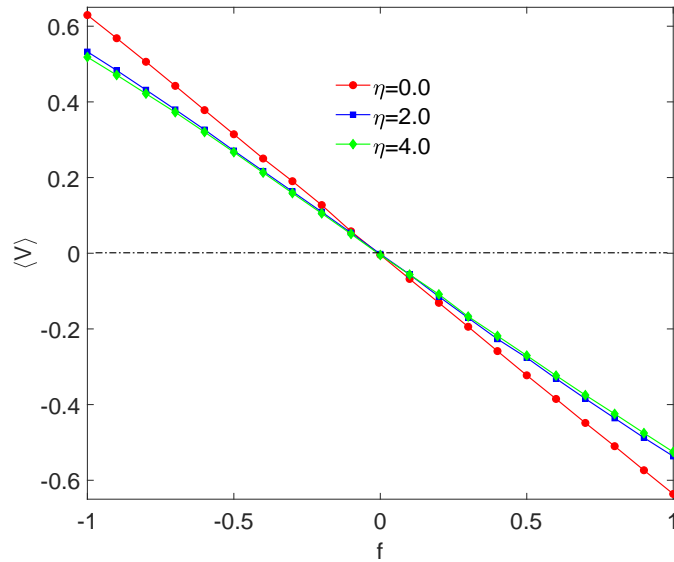


Fig. 13. The average velocity $\langle V \rangle$ as a function of load f for different η . The other parameters are $\Delta = 0.8$, $\varepsilon = 0.5$, $v_0 = 0.5$, $Q_x = Q_y = Q_\theta = 1.0$, $\tau_x = \tau_y = \tau_\theta = 1.0$.

The average velocity $\langle V \rangle$ as a function of the load f for different η is reported in Fig.13. We find $\langle V \rangle$ decreases monotonically with increasing load f . $\langle V \rangle > 0$ when $f < 0$, but $\langle V \rangle < 0$ when $f > 0$. This means negative load leads to positive transport(directed transport in $-x$ direction), but positive load leads to negative transport. Directed transport speed $|\langle V \rangle|$ increases with increasing $|f|$, so large load $|f|$ is good for directed transport(in x direction or in $-x$ direction). We know the potential U is inversely proportional to the load f (Fig.2), so the particles move to the place where potential is lower. In this figure, we can also find the smaller η , the larger $|\langle V \rangle|$ is.

4. Conclusions

In this paper, we numerically investigated the directed transport of self-propelled ellipsoidal particles confined in a smooth channel with potential and colored noise. We find the moving direction is closely linked to the direction of the load when the self-propelled speed is small ($v_0 < 3$). Negative load leads to directed transport in x direction, but positive load leads to directed transport in $-x$ direction. Small and large size of bottleneck restrains the directed transport of the ellipsoidal particle. Large x axis noise intensity inhibits the directed transport. But proper value of y axis noise intensity is good for this phenomenon. The transport reverse phenomenon appears with increasing self-propelled speed v_0 . The effects of angle noise on the system is negligible.

Acknowledgments

Project supported by Natural Science Foundation of Anhui Province (Grant No:1408085QA11).

1. P. Hänggi, F. Marchesoni, *Rev. Mod. Phys.* **81** 387 (2009).
2. P. S. Burada, P. Hänggi, F. Marchesoni, G. Schmid, P. Talkner, *Chem. Phys. Chem.* **10** 45 (2009).
3. H. X. Zhou, G. N. Rivas, A. P. Minton, *Annu. Rev. Biophys.* **37** 375 (2008).
4. Y. Wu, Q. Ding, T. Li, D. Yu, Y. Jia, *Nonlinear Dynamics* **111** 2693 (2023).
5. J. Liu, J. D. Bao, X. Chen, *Phys. Rev. E* **102** 062122 (2020).
6. R. F. Cui, Q. H. Chen, J. X. Chen, *Nanoscale* **12** 12275 (2020).
7. F. J. Keil, R. Krishna, M. O. Coppens, *Rev. Chem. Eng.* **16** 71 (2000).
8. M. Firnkes, D. Pedone, J. Knezevic, M. Döblinger, U. Rant, *Nano. Lett.* **10** 2162 (2010).
9. D. Pedone, M. Langecker, G. Abstreiter, U. Rant, *Nano. Lett.* **11** 1561 (2011).
10. Z. Siwy, A. Fulinski, *Am. J. Phys.* **72** 567 (2004).
11. Z. Siwy, I. D. Kosinska, A. Fulinski, C. R. Martin, *Phys. Rev. Lett.* **94** 048102 (2005).
12. L. Bosi, P. K. Ghosh, F. Marchesoni, *J. Chem. Phys.* **137** 174110 (2012).
13. P. K. Ghosh, V. R. Misko, F. Marchesoni, F. Nori, *Phys. Rev. Lett.* **110** 268301 (2013).
14. S. Matthias, F. Müller, *Nature* **424** 53 (2003).
15. T. M. Squires, S. R. Quake, *Rev. Mod. Phys.* **77** 977 (2005).
16. R. M. Bradley, *Phys. Rev. E* **80** 061142 (2009).
17. L. Dagdug, I. Pineda, *J. Chem. Phys.* **137** 024107 (2012).
18. Y. Jia, S. N. Yu, J. R. Li, *Phys. Rev. E* **63** 052101 (2001).
19. C. Hu, Y. Ou, J. Wu, Q. Chen, B. Ai, *J. Stat. Mech.* **2015** 05025 (2015).
20. Z. Liu, L. Du, W. Guo, D. C. Mei, *Eur. Phys. J. B* **89** 222 (2016).
21. Y. Xu, Y. Jia, M. Ge, L. Lu, L. Yang, X. Zhan, *Neurocomputing* **283** 196 (2018).
22. H. W. Hu, L. Du, L. H. Qu, Z. L. Cao, Z. C. Deng, Y. C. Lai, *Phys. Rev. Research* **3** 033162 (2021).
23. J. Richardi, M. P. Pileni, J. J. Weis, *J. Chem. Phys.* **130** 124515 (2009).
24. Z. Yoshida, H. Saitoh, J. Morikawa, Y. Yano, S. Watanabe, Y. Ogawa, *Phys. Rev. Lett.* **104** 235004 (2010).
25. P. K. Ghosh, F. Marchesoni, S. E. Savelev and F. Nori, *Phys. Rev. Lett.* **104** 020601 (2010).

14 BING WANG

26. P. K. Ghosh, R. Glavey, F. Marchesoni, S. E. Savelev, F. Nori, *Phys. Rev. E* **84** 011109 (2011).
27. P. Hänggi, F. Marchesoni, S. Savelev, G. Schmid, *Phys. Rev. E* **82** 041121 (2010).
28. P. K. Ghosh, P. Hänggi, F. Marchesoni, F. Nori, G. Schmid, *Phys. Rev. E* **86** 021112 (2012).
29. J. X. Chen, Y. G. Chen, R. Kapral, *Advanced Science* **1800028** (2018).
30. M. Pu, H. Jiang, Z. Hou, *Soft Matter* **13** 4112 (2017).
31. Y. Li, F. Marchesoni, D. Debnath, P. K. Ghosh, *Phys. Rev. Res.* **1** 033003 (2019).
32. X. Yang, Q. Zhu, C. Liu, W. Wang, Y. Li, F. Marchesoni, P. Hänggi, H. P. Zhang, *Phys. Rev. E* **99** 020601(R) (2019).
33. P. G. Saffman, M. Delbruck, *Proc. Natl. Acad. Sci. U.S.A.* **72** 3111 (1975).
34. F. Lugli, E. Brini, F. Zerbetto, *J. Chem. Phys. C* **116** 592 (2012).
35. Y. Han, A. M. Alsayed, M. Nobili, J. Zhang, T. C. Lubensky, A. G. Yodh, *Science* **314** 626 (2006).
36. T. Ohta, T. Ohkuma, *Phys. Rev. Lett.* **102** 154101 (2009).
37. B. Ai, J. Wu, *J. Chem. Phys.* **140** 094103 (2014).
38. P. K. Ghosh, P. Hänggi, F. Marchesoni, F. Nori, *Phys. Rev. E* **89** 062115 (2014).
39. S. Zhu, A. W. Yu, R. Roy, *Phys. Rev. A* **34** 4333 (1986).
40. X. Zhou, *Phys. Rev. A* **80** 023818 (2009).
41. K. Y. R. Billah, M. Shinozuka, *Phys. Rev. A* **42** 7492 (1990).
42. R. Wittmann, J. M. Brader, A. Sharma, U. Marini Bettolo Marconi, *Phys. Rev. E* **97** 012601 (2018).
43. S. Mondal, B. C. Bag, *Phys. Rev. E* **91** 042145 (2015).
44. R. Grima, S. N. Yaliraki, and M. Barahona, *J. Phys. Chem. B* **114** 5380 (2010).
45. P. K. Ghosh, *J. Chem. Phys.* **141** 061102 (2014).